Accepted Manuscript

Impact response and energy absorption of single phase syntactic foam

Thong M. Pham, Wensu Chen, Jim Kingston, Hong Hao

PII: S1359-8368(18)30893-X

DOI: 10.1016/j.compositesb.2018.05.057

Reference: JCOMB 5727

To appear in: *Composites Part B*

Received Date: 19 March 2018

Revised Date: 28 May 2018

Accepted Date: 30 May 2018

Please cite this article as: Pham TM, Chen W, Kingston J, Hao H, Impact response and energy absorption of single phase syntactic foam, *Composites Part B* (2018), doi: 10.1016/j.compositesb.2018.05.057.

Impact Response and Energy Absorption of Single Phase Syntactic Foam

Thong M. Pham[1], Wensu Chen[2], Jim Kingston[3], and Hong Hao[4]

Abstract

This study experimentally investigates the static and impact response of a new single phase syntactic foam which has been newly developed for impact energy absorption. The syntactic foam had different densities ranging from 172 kg/m^3 to 366 kg/m^3 depending on the thickness and composition of the coating layers. The impact response and impact energy absorption were investigated by using instrumented drop-weight impact tests. Under static loads, the mechanical properties of the syntactic foam including the compressive strength, the yield stress, and Young's modulus increased with the density but the rate of increment decreased at higher densities. There were two types of progressive failures of the syntactic foam under impact loads. The failure propagation was examined and found to be dependent on the material density and the impact velocity. Interestingly, the densification only occurred in the low-density specimens while this phenomenon was not observed for the specimens with the density greater than 288 kg/m^3. The impact energy absorption capacity increased significantly with the density and the wall thickness of the macrospheres.

Keywords: Single phase syntactic foam; Impact loading; Energy absorption; Densification.

[1]Research Fellow, Center for Infrastructural Monitoring and Protection, School of Civil and Mechanical Engineering, Curtin University, Kent Street, Bentley, WA 6102, Australia (corresponding author). Email: thong.pham@curtin.edu.au

[2]Senior Research Fellow, Center for Infrastructural Monitoring and Protection, School of Civil and Mechanical Engineering, Curtin University, Kent Street, Bentley, WA 6102, Australia. Email: wensu.chen@curtin.edu.au

[3]Product Line Manager, Matrix Composites & Engineering, 150 Quill Way, Henderson, WA 6166, Australia. Email: jim.kingston@matrixengineered.com

[4]John Curtin Distinguished Professor, Center for Infrastructural Monitoring and Protection, School of Civil and Mechanical Engineering, Curtin University, Australia, and School of Civil Engineering, Guangzhou University, China (corresponding author). Email: hong.hao@curtin.edu.au.

Introduction

Syntactic foam made of engineered composite spheres is a type of porous material with good crush strength and energy absorption capacity, which has attracted an increasing interest and attention from scientific and engineering communities. The syntactic foam material can be used for engineering applications across a range of industries such as mining, marine, transportation, civil, defence and aerospace in lieu of its characteristics of low density, good thermal efficiency, high strength-to-weight ratio and impact resistance capacity [1]. The specific applications include road barriers, sandwich structure, open pit edge protection and aerospace structure [2, 3] etc. By applying the syntactic foam material for the roadside barrier, the impact force can be significantly reduced while the energy absorption capacity remains [4]. Sandwich structure made of syntactic foam as core material can be used as protective layers for vehicles against impact and blast loads [5]. In open pit mines, the syntactic foam material can be applied to the edge protection, which allows the narrower open pit haul roads while remaining the safety requirement for trucks [6]. For marine applications, the syntactic foam is able to provide buoyancy due to its light weight and withstand high water pressure for deep-sea exploration [7, 8] .

Syntactic foam is a kind of composite material which can be classified into one-phase, two-phase and three-phase foams [7, 9]. Typical syntactic foam consists of filler and a binder matrix. The fillers can be made of glass, metal, ceramic, cenosphere in the forms of micro-sphere or macro-sphere [10-12]. The binder matrix can be made of polymeric binders and metals [13-15]. One-phase foam is formed by bonding engineered composite sphere matrix, which is made from EPS (Expanded Polystyrene) beads coated with epoxy resin matrix or fibre reinforced epoxy using “rolling ball method” [7, 16]. The coated EPS beads can be cured and post-cured to shrink the EPS beads inside the spheres to produce hollow structures.

The hollow engineered composite spheres are then bonded and form into one-phase foam. Without curing process, the EPS beads can be also unshrunk and fill inside the spheres, which is a variant of one-phase foam. To improve the mechanical properties of syntactic foam, the micro-spheres and macro-spheres made of various fillers can be added and mixed with binder matrix to form two-phase and three-phase syntactic foams [10, 11]. Zhi et al. [17] investigated the interfacial bond properties of syntactic foam made of fibres, fillers and matrix using microbond test and numerical simulation. It was found that the fibre diameter has the largest effect on the interfacial shear strength of syntactic foam, followed by the volume fraction and size of the fillers.

The mechanical properties of syntactic foam material have been reported in the literature. The syntactic foam material shows superior mechanical properties in lieu of the composite action by filler and matrix. The compressive stress of homogenous EPS (Expanded Polystyrene) only foams with density of 13.5 kg/m^3 and 28 kg/m^3 at 10% strain are 0.089 MPa and 0.191 MPa, respectively [18], which is well below the compressive strength of normal syntactic foam. As reported by Swetha and Kumar [10], the strength of the syntactic foam decreased with the increase in microsphere content. The energy absorption capacity peaked when the content of microsphere was up to 40%. As observed by Kim and Khamis [19], the impact performance enhanced while the fracture toughness and flexural strength decreased with the increasing volume fraction of the microsphere in the syntactic foam. However, Wouterson et al. [20] reported the opposite results, i.e. the existence of the microsphere of syntactic foam improved the fracture toughness while decreased the impact resistance capacity. Further studies have shown that particles of very thin walls lead to decease in properties as the particle volume fraction is increased. However, above a critical wall thickness, increase in particle fraction leads to improved syntactic foam properties [2]. To improve the mechanical behaviour and enhance impact energy absorption capacity, crumb rubber has been added into

syntactic foam [21-23]. It was found that the optimal volume fraction of the crumb rubber ranged between 10% and 20% in terms of fracture toughness. The effect on its energy absorption capacity and fracture toughness by adding crumb rubber into the syntactic foam was investigated under quasi-static and impact loads in the previous study [9]. It should be noted that syntactic foam as lightweight composites has many applications and dynamic behaviours of syntactic foam material are worth studying due to its great potential applications in impact resistance and protection against extreme loads. Syntactic foam can be pre-cast in factories or cast in-situ to almost any common shapes. For instance, this material has been used to fill in the edge protectors for vehicles in the previous study by Durkin et al. [6] and this application has been used in mines in Western Australia.

In the existing literature, dynamic properties of syntactic foams and/or polymeric foams have been experimentally investigated. For instance, Song et al. [24] investigated mechanical properties of epoxy syntactic foam at intermediate strain rate by using modified MTS material tester and modified split Hopkinson pressure bar (SHPB). It was reported that the failure strength of syntactic foam exhibited strain-rate dependency. Li et al. [25] conducted the compressive tests on glass micro balloon syntactic foams by using hydraulic loading machine for medium strain rate and SHPB for high strain rate up to 4000 s^{-1}. The stress-strain response was obtained and the compressive properties exhibited strain rate dependency. Additionally, the microscopic observations from testing combined with numerical simulations revealed failure mode and failure mechanism of syntactic foam. Ouellet et al. [26] also investigated the compressive properties of polymeric foams under quasi-static, medium and high strain rate by using SHPB. It was found that the strain rate effects became pronounced at the rate above 1000 s^{-1}. Peter and Woldesenbet [27] investigated the effect of nanoclay on the high strain rate mechanical properties of syntactic foams. The high strain rate tests were conducted by using SHPB. The authors found that the inclusion of 1% nanoclay volume fraction yield the

optimum enhancement in peak stress and modulus of nanoclay syntactic foam properties. Viot et al. [28] examined the material properties of syntactic foam under high rate loadings. The effects of the microsphere volume fraction, projectile mass, and drop height on the energy absorption were investigated. The authors observed significant effects of the microsphere volume fraction and drop height and marginal influence of the projectile mass on the energy absorption. The energy absorption mechanism includes the visco-plastic deformation of the matrix and the fracture of the glass bubble structure. The failure of the glass bubble mainly governed the energy absorption when its volume fraction was high while the resin deformation primarily controlled the energy absorption of low volume fraction syntactic foams. In addition, Shams et al. [29] developed a micromechanical model for the simulation of syntactic foams under high strain rate loads. The proposed numerical model enables the predication of syntactic foam behaviour at a wide range of strain rates and various micro balloon configurations. The above-mentioned existing experimental and numerical studies on the dynamic properties of various syntactic foams can be referred for the dynamic properties investigations of new single-phase syntactic foam proposed in this study.

This study aims to propose a new single-phase syntactic foam with high energy absorption capacity. The effects of material density and wall thickness of spheres on both the strength and energy absorption are examined for the purpose of deriving the optimal material designs for various applications. In this paper, the mechanical behaviours of four types of single-phase syntactic foam materials (with four densities of 172, 288, 318, and 366 kg/m^3) were investigated subjected to quasi-static and impact loads. The specimens were made of the same mother materials but they had different coating layers which result in varied densities. The mechanical properties and static/impact energy absorption of the syntactic foams were experimentally examined. Furthermore, different types of the failure propagation under impact tests were discussed based on quantitative analyses and analytical solutions.

Specimen manufacturing

In this study, the single phase syntactic material was prepared and fabricated by the company Matrix, Australia [30]. The syntactic foam was made of engineered composite macro-spheres. The macro-spheres were formed from spherical, low density EPS (Expanded Polystyrene) beads coated using rolling ball method [7, 16] with layers of short-fibre reinforced composite, which is a combination of mineral fibre (i.e. wollastonite) and epoxy resin as shown in Fig. 1. The compressive strength and modulus of the epoxy resin were 100 MPa and 2750 MPa, respectively. After applying multiple coats of short-fibre reinforced composite, the macro-spheres were extracted from the process followed by a final coating of epoxy resin without mineral fibre. The sticky (for fingers) macro-spheres with certain viscosity were then poured into a suitable cavity based upon the volume of resin and the estimated macro-sphere surface area. In this study, the packing density was 60% as a feature of randomly packed spherical particles [31]. After that, the epoxy resin was cured at 60^0C for 4 hours to set the material into its final form. It is worth noting that the epoxy-coated macro-spheres can be cured to shrink the EPS beads inside the macro-spheres to produce hollow macro-sphere structures. The hollow macro-spheres, which had the average diameter of 3.5 mm and coating thickness of 35.1~40.1 μm, were evenly distributed in the foam. The varying coating thicknesses are corresponding to different densities. The syntactic foam was estimated to have a density of 172~366 kg/m3. It is noted that the density, strength and stiffness of macro-spheres and syntactic foam can be tailored to meet with the requirements of various applications.

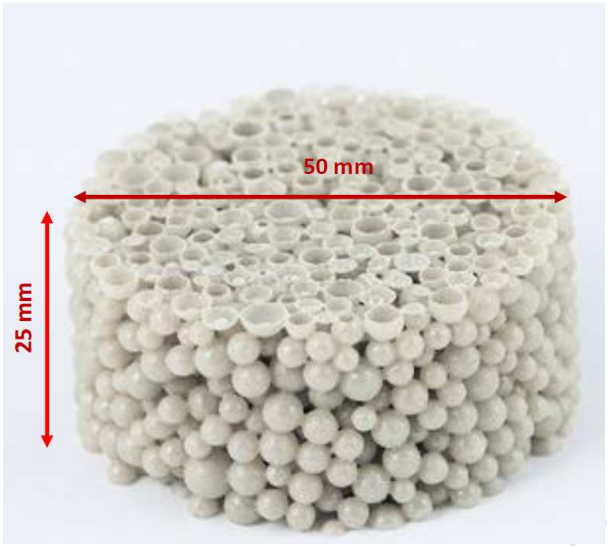

Figure 1 Single-phase syntactic foam material

The mechanical properties of the single phase foam were investigated under static and impact loads. There were two sizes of cylindrical specimens in this study including ϕ100x180 mm for the impact tests and ϕ50x100 mm for the static tests. These specimens had varied densities, which were 172 kg/m^3, 288 kg/m^3, 318 kg/m^3, and 366 kg/m^3, resulted from different coating layers and thicknesses. As mentioned previously, the specimens could have the EPS beads shrunk or fully filled in the spheres, depending on the different curing processes.

Static mechanical properties

The compressive strength of the one phase syntactic foam was investigated by conducting standard compression tests. The tested cylinders had the diameter of 50 mm and the height of 100 mm. There were four different groups with different densities which were considered in the static tests. Each group contained five identical specimens which had the densities of 172 kg/m^3, 288 kg/m^3, 318 kg/m^3, and 366 kg/m^3, respectively. These specimens were prepared in separate molds with the same dimension. The stress-strain curves of the tested cylinder are presented in Figs. 2-4 and the test results are presented in Table 1. The stress-strain curves of the tested specimens were linear up to the yielding points before fluctuating around their

maximum stress. After reaching the yielding points, stress of the specimens dropped owing to the crushing of one layer of coated EPS spheres. The progressive failure of one layer of coated EPS spheres led to a local reduction of the stress-strain curves. The stress of the specimens then increased again when the damaged layer reached the densification level of the material. The progressive failure of the specimens continued until very large deformation and the compression tests were stopped at the axial strain of 35% because of the limit of the testing machine.

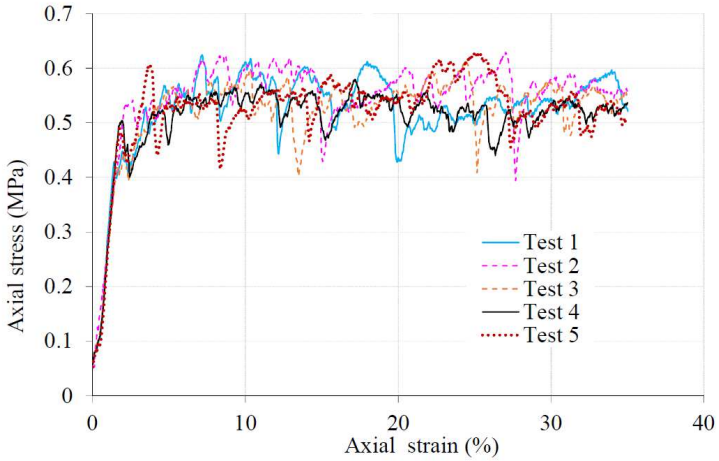

Fig. 2. Stress-strain relationship of the single phase syntactic foam (ρ = 172 kg/m^3)

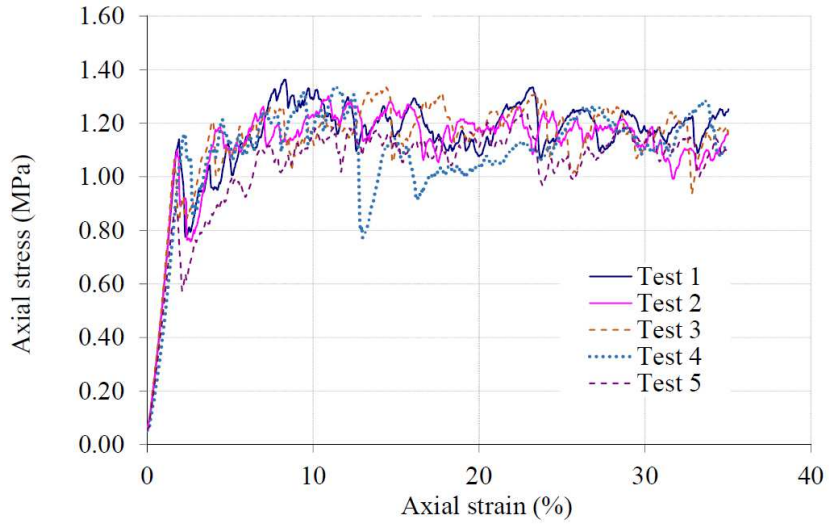

Fig. 3. Stress-strain relationship of the single phase syntactic foam (ρ = 288 kg/m^3)

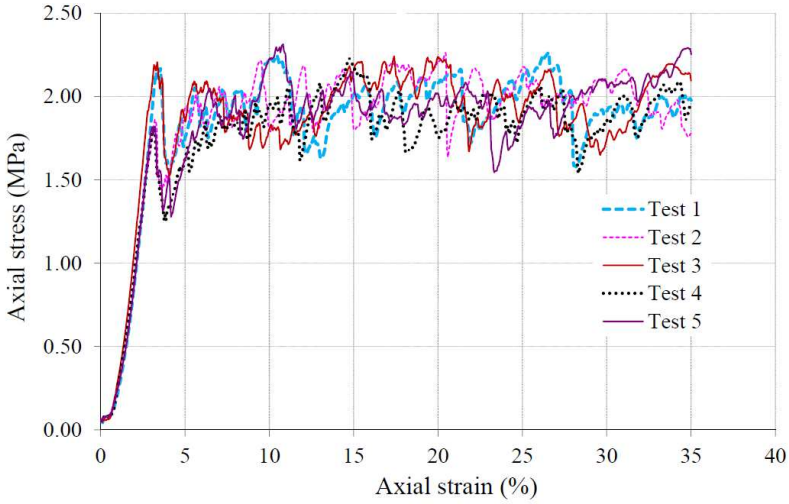

Fig. 4. Stress-strain relationship of the single phase syntactic foam (ρ = 366 kg/m^3)

In addition, the yield strain of these specimens did not show a considerable variation among the tested specimens with density between 172 and 366 kg/m^3. The yield strain of the specimens was 0.89%, 1.10%, 1.05%, and 1.58% corresponding to the densities of 172 kg/m^3, 288 kg/m^3, 318 kg/m^3, and 366 kg/m^3, respectively. On the other hand, the yield stress increased significantly with the density of the specimens with the yield stress of 0.51 MPa, 1.14 MPa, 1.41 MPa, and 1.91 MPa, respectively. Consequently, the maximum stress of the specimens also increased significantly with the material density. The Young's modulus of the material increased significantly from 63 MPa to 119 MPa when the density changed from 172 kg/m^3 to 288 kg/m^3. However, the rate of increase in Young's modulus of the material with further increase in density slowed down with 119 MPa for ρ = 288 kg/m^3 to 142 MPa for ρ = 366 kg/m^3. Besides, the energy absorption computed by the area under the load-displacement curves is also presented in Table 1. Briefly, the yield strain, yield stress, Young's modulus, and energy absorption varied in a different manner with the change in coating and density. Thus, a desirable character can be achieved and designed based on the experimental results as above.

The average plateau stress of these foam can be estimated by adopting an empirical model. The plateau stress (σ_{pl}) related to relative density ($\frac{\rho}{\rho_s}$) can be described by the following form [32].

$$\frac{\sigma_{pl}}{\sigma_{y,s}} = \alpha \left(\frac{\rho}{\rho_s}\right)^{1.5} \quad (1)$$

where σ_{pl} - plateau stress; $\sigma_{y,s}$ - strength of epoxy resin; ρ - density of the foam; ρ_s -density of the epoxy resin; and α is the coefficient to be calibrated from the experimental results. In this study, the strength of epoxy resin was 100 MPa. The density of the epoxy resin was about 1150 kg/m^3. The density of the foams were 172 kg/m^3, 288 kg/m^3 and 366 kg/m^3, respectively.

Under quasi-static load, the foams with the density of 172 kg/m^3, 288 kg/m^3 and 366 kg/m^3 had the average plateau stress (σ_{pl}) of 0.55 MPa, 1.10 MPa and 1.90 MPa, respectively, as shown in Figs. 2-4. The coefficient for the single phase syntactic foam was 0.096. The ratio of plateau stress to epoxy strength ($\frac{\sigma_{pl}}{\sigma_{y,s}}$) can be well predicted by the empirical formula $\frac{\sigma_{pl}}{\sigma_{y,s}} = 0.096 \left(\frac{\rho}{\rho_s}\right)^{1.5}$. The predicted average plateau stresses for the foams with the density of 172 kg/m^3, 288 kg/m^3 and 366 kg/m^3 are 0.56 MPa, 1.20 MPa and 1.72 MPa, respectively.

Impact response

Drop-weight tests

The instrumented drop-weight tests were utilized to investigate the impact behavior of the single phase syntactic foam. The drop-weight apparatus included a solid steel projectile which was dropped from the designated height to the top of the specimens. There were two steel projectiles used in this study, including the heavy projectile weighing 100 kg and another

light projectile of 28.26 kg as shown in Fig. 5. The heavy projectile had a smooth flat bottom with a radius of 50 mm while the light projectile was steel cylinder with the radius of 75 mm and flat bottom. The heavy projectile was used in the test of most of the specimens except Specimen 172_3 which was impacted by the light projectile. The small projectile was used to investigate the effect of higher impact velocity by dropping from a greater height. The projectiles were falling onto the specimen top within a plastic guiding tube as shown in Fig. 6. The specimens were placed on the top of a load cell which was used to measure the impact force and was fixed on a strong floor. The reason to place the load cell at the bottom of the specimens was explained in the study by Pham and Hao [33]. A high-speed camera, which was set to capture 50400 frames per second, was used to monitor the failure processes, displacements, velocities, and accelerations of the projectile and the specimens. The above frame rate was chosen based on the experiences from the previous study in which lower frame rate was not able to sufficiently capture the failure process. The data acquisition system recorded data at a sampling rate of 1 MHz as recommended in the previous study by Pham and Hao [33]. In the latter study, the authors investigated the effect of different sampling rates on the recorded data and suggested that a sampling rate less than 1 MHz may not yield accurate results in this circumstance.

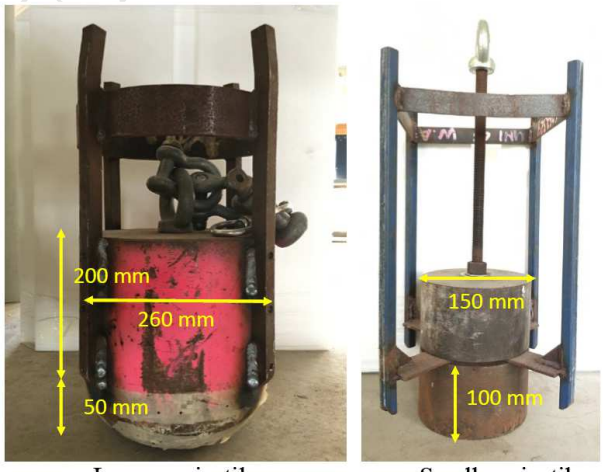

Fig. 5. Shape of the two steel projectiles

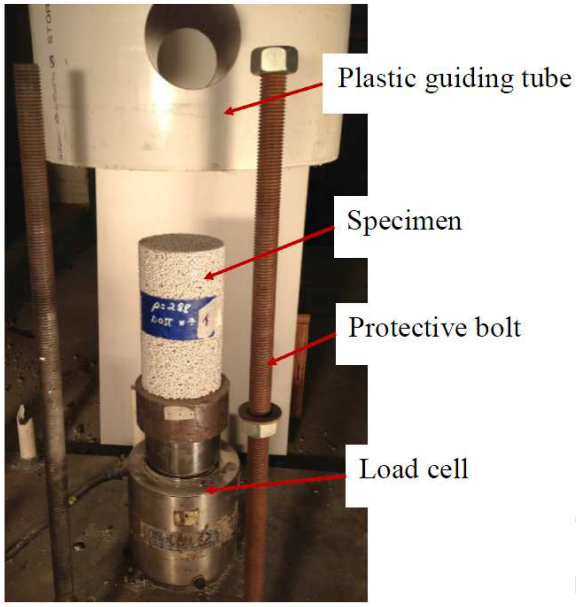

Fig. 6. Drop-weight test apparatus

Failure propagation and stress evolution

There were two different types of the failure propagation observed in the testing. The first failure mode, which was observed when testing specimens with light density (ρ = 172 or 288 kg/m^3), initiated from the bottom of the specimens and propagated upward to the top of the specimens. These specimens were tested under varying drop heights from 0.63, 0.95 to 1.29 m. The top of the specimens was not damaged until the end of the impact events as shown in Fig. 7. The whole impact duration was about 60-80 milliseconds for all the specimens. The second failure mode occurred with higher density specimens (ρ = 366 kg/m^3, drop heights from 0.95-1.29 m), for which failure also initiated at the bottom but the failure soon occurred at the top about 2-3 ms later. The failure then propagated to the midheight from both ends as shown in Fig. 8. The failure propagation of the specimens with density of 318 kg/m^3 showed a mixed modes of the failure propagation. The difference in the failure mode can be explained by the stress evolution in these specimens. The stress evolution was estimated based on a solution presented by Johnson [34] and adopted by Pham et al. [35].

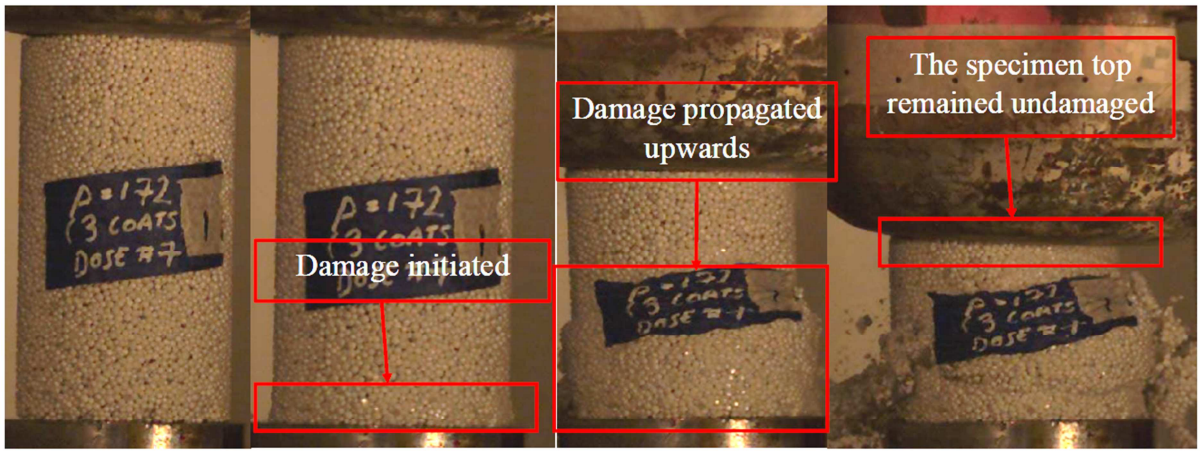

Fig. 7. Progressive failure of Specimen 172_1

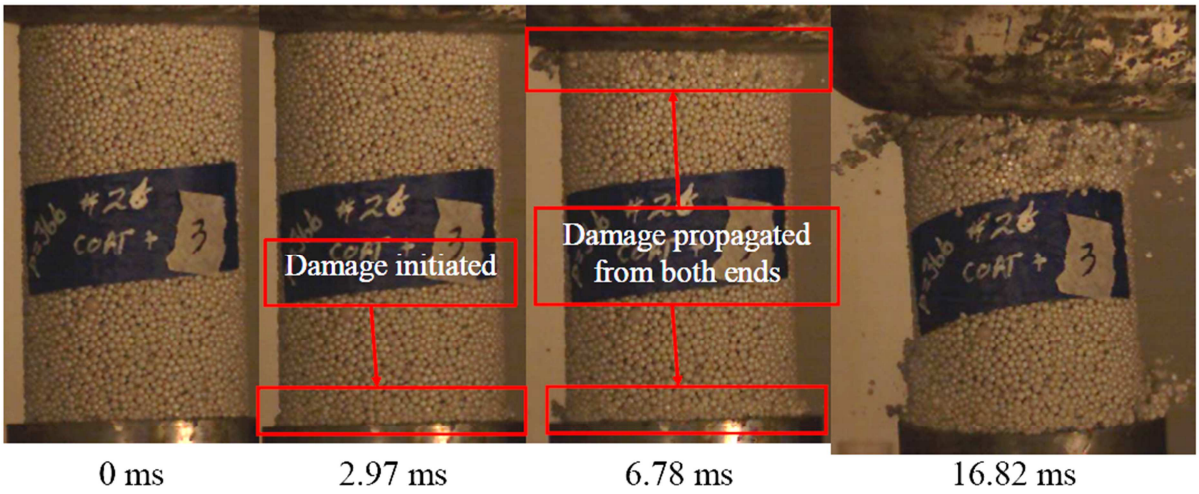

Fig. 8. Progressive failure of Specimen 366_3

The analytical solution examined the stress evolution of a short cylinder on a frictionless flat rigid base. The rigid projectile impacts the cylinder from the top with a speed *V*. The stress evolution in the cylinder is dependent on the elastic and plastic wave speeds, the material properties, and the impact velocity. The wave speeds can be estimated as follows:

$$c_0 = \sqrt{\frac{E}{\rho_0}} \tag{2}$$

$$c_1 = \sqrt{\frac{P}{\rho_0}} \tag{3}$$

where c_0 and c_1 are the elastic and plastic wave speeds, respectively, E and P are respectively Young's modulus and the plastic modulus of the material, and ρ_0 is the density of the material in its unstrained state. The stress wave propagation and the stress evolution in the specimens are presented in Fig. 9. It is noted that Y is the yield stress of the material. Based on the analytical solution and the material properties, the stress evolution of the tested specimens is calculated and shown in Fig. 10. As shown in the figure, when the projectile impacted the specimens, the stress at the top of the specimens was smaller than the material strength and thus did not cause any damage to the specimens at the early instant. Accordingly, stress at the bottom of the specimens (Zone 2) initiated the damage of all the specimens as described in Fig. 10, for example, the stress in Zone 2 of Specimens 172, 288, and 366 was 0.63 MPa, 1.38 MPa, and 2.51 MPa which were greater than the material strength (from static tests: 0.61 MPa, 1.30 MPa, and 2.26 MPa), respectively. A quantitative analysis was carried out to explain why these specimens failed in different manners. It is noted that the stress evolution in these specimens is estimated based on the equations presented in Fig. 9 and more details about the derivation of these equations can be found in the study by Johnson [34].

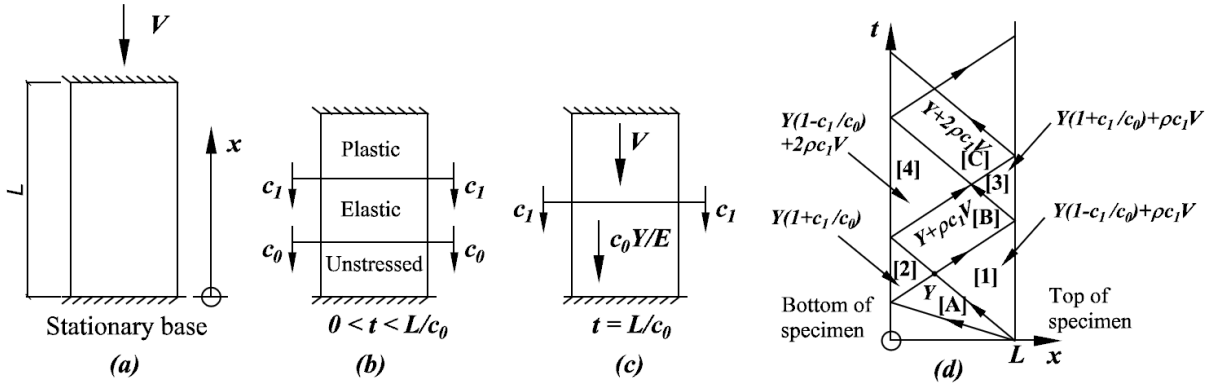

Fig. 9. Stress evolution mechanism under impact

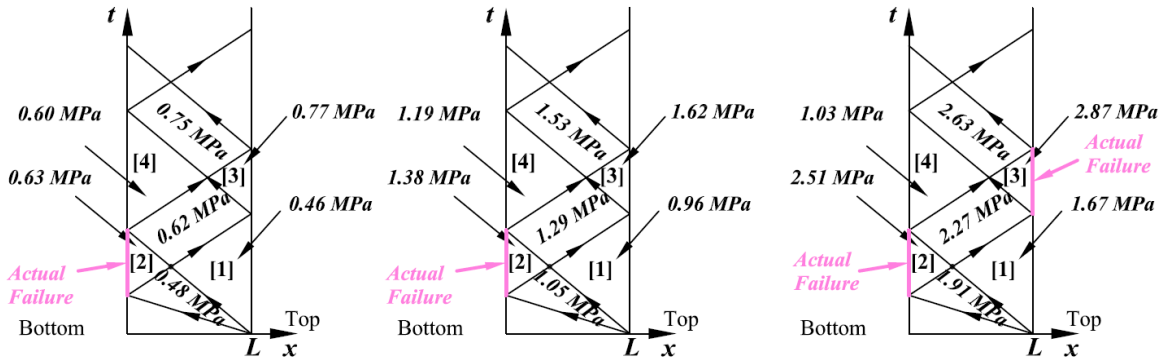

Fig. 10. Stress evolution of the tested specimens

After the failure initiation, the progressive damage of the tested specimens was different as mentioned previously. The specimens with low density (ρ < 288 kg/m^3) showed the damage started and propagated from the bottom upwards while the specimen top remained undamaged before the end of impact events. Meanwhile, the three specimens in Group 366 exhibited a consistent failure mode in which the damage simultaneously propagated from the top and bottom towards the midheight of the specimens. There are two possible reasons for this variation of the failure mode. Firstly, specimens with low density (ρ < 288 kg/m^3) showed a high level of densification as shown in Fig. 7 while Specimens 366 did not show a high level of densification since the failed fragments flew out as shown in Fig. 8. The damage of the low-density specimens absorbed relatively more impact energy normalized with its density

than those of Specimens 366. As a result, there was weaker reflected stress wave to form stress at Zone 3 (Fig. 9) of the low-density specimens than that of Specimens 366 according to the corresponding coming stress wave. The high level of the densification of the low-density specimens, which led to the damage just propagated from the bottom upwards, is also shown in the impact force time histories (presented in the following section). Secondly, because of the nature of the material and the impact velocity, the stress at Zone 3 of these specimens is different. The increase of the stress in Zone 3 compared to that in Zone 2 shows the vulnerability of a specimen to damage at the top after the failure of the bottom. It means that the smaller difference between the stresses in Zone 3 compared to Zone 2, the easier to show damage in Zone 3. In Fig. 10, for instance, the difference between Zone 3 and Zone 2 of Specimens 172 ((0.77-0.63)/0.63 = 22%) is greater than that of Specimens 366 ((2.87-2.51)/2.51 = 14%). This progressive failure of the single syntactic foam is obviously different from the failure of concrete material, for instance, Pham and Hao [33] presented similar impact tests on concrete cylinders and the concrete specimens always failed at the impact end associated with the first drop.

Impact force time histories

Impact force time histories of the tested specimens were derived from the load cell record and presented in Figs. 11-13. It is noted that the impact forces from the specimens which were not shown in these figures were lost owing malfunction of the data acquisition system during testing. The impact force time history of Specimen 172_2 (Fig. 11) showed a constant impact force at about 7.5 kN for a duration of approximately 40 ms (from 90 ms to 130 ms). During this period, the progressive failure occurred while the densification did not exist. However, the densification appeared afterward and led to a significant increase of the impact force up to 27 kN, which confirms the above explanation of the high level of densification of the low-

density specimens. On the other hand, the impact force time histories of higher-density specimens did not show a densification process (Figs. 12-13) in which the impact force of Specimens 288 and 366 did not show a considerable difference. It means that increasing the density (from 288 kg/m^3 to 366 kg/m^3) did not lead to an enhancement of the impact force. The impact force of these specimens reached the peaks of about 10-15 MPa, then fluctuated around 8-10 MPa before dropping to zero.

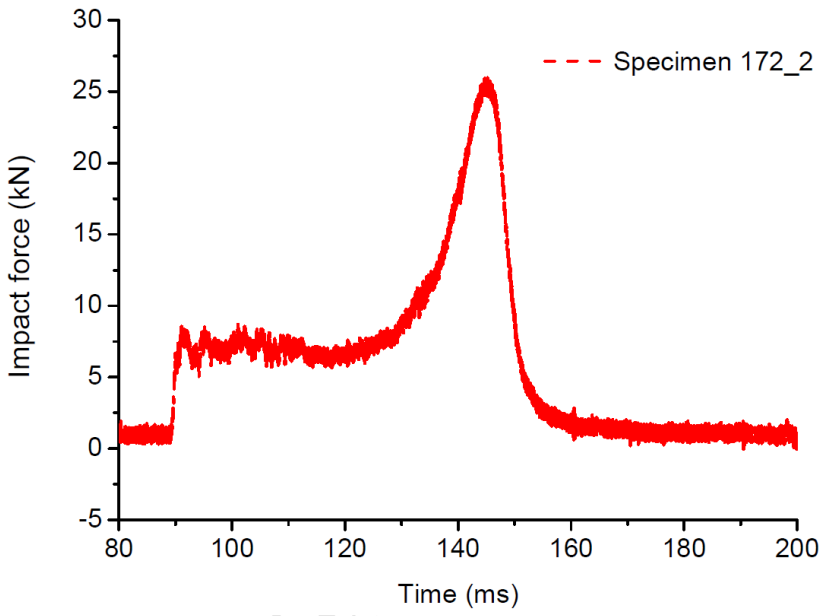

Fig. 11. Impact force time history of Specimen 172_2

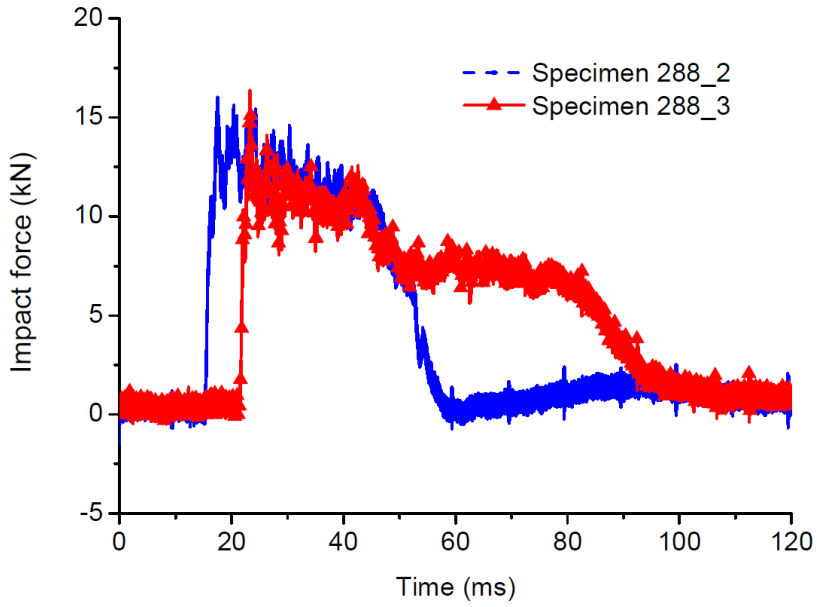

Fig. 12. Impact force time histories of Specimens 288

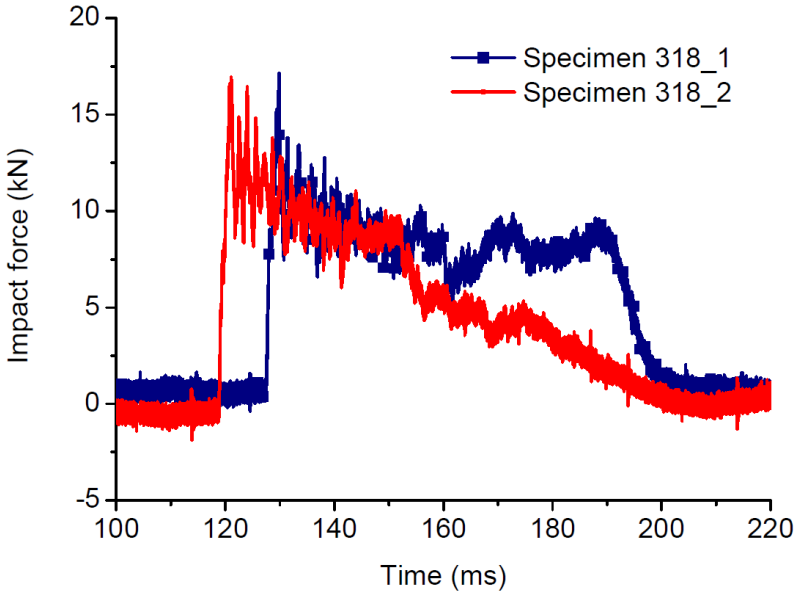

Fig. 13. Impact force time histories of Specimens 318

To examine the dynamic compressive strength of the tested specimens, the compressive stress was calculated from the impact force time histories and presented in Fig. 14. It is interesting that the dynamic strength of all the tested specimens was not much different from that under static tests with the exception of Specimen 172_2 after the densification. This response is beneficial when the material is used as a sacrificed layer in protective structures. For example, if this material with density of 318 kg/m^3 is used in a sacrificed layer, its peak dynamic stress is greater than 2 MPa and then reduces to a plateau of about 1 MPa which is even smaller than the static strength. This response will reduce the impact force that transfers from a collision to the protected structures. The excellent ability of absorbing impact energy is confirmed from the tests since this material was able to stop 100 kg projectile dropping from 1.3 m (result in 1.3 kJ impact energy) while the similar impact energy cannot be absorbed by a similar size concrete cylinder with the compressive strength of 46 MPa as presented by Pham and Hao [33]. In the same test setup and specimen size, the residual velocity of the projectile was zero

for some specimens in this study while the corresponding residual velocity was greater than zero after impacting the concrete specimens as reported by Pham and Hao [33].

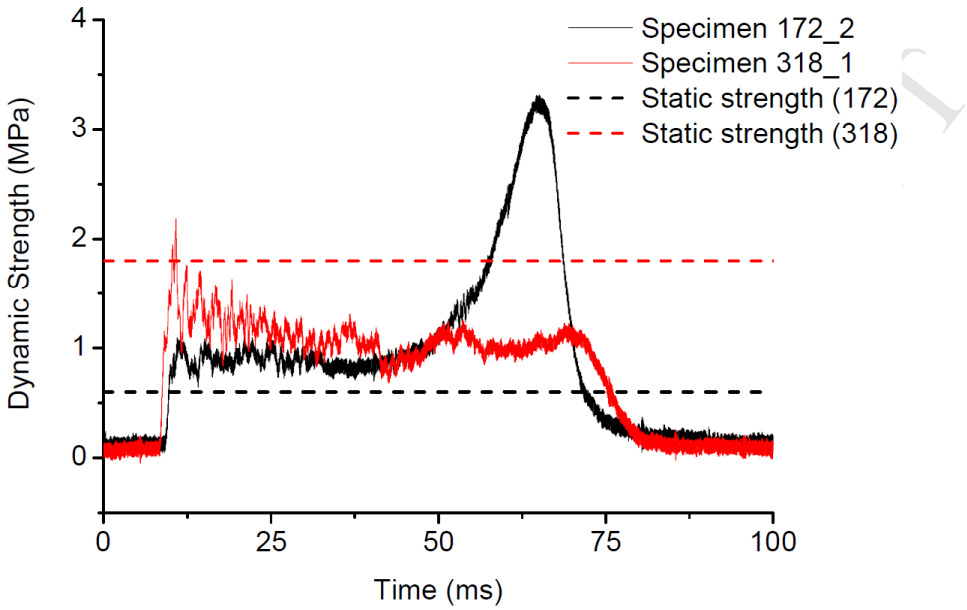

Fig. 14. Impact forces vs static strengths

Energy absorption

The energy absorption capacity of the tested specimens is investigated from the impact energy and the residual energy. The impact energy is the kinetic energy of the projectile just prior to the impact event and is calculated from the impact velocity and the projectile weight. The residual energy is estimated from the projectile weight and the residual velocity which has two possibilities including rebounding velocity and residual velocity. The rebound velocity is in the opposite direction to the impact velocity so that it is negative. The testing results and the energy absorption of the tested specimens are presented in Table 2.

It is obvious that specimens with EPS fully filling the macro spheres show better ability to absorb impact energy. For example, Specimen 288_1 absorbed 1.3 kJ and the specimen was totally damaged while the specimen 288b_1 was completely damaged with the energy of 0.8

kJ. It is noted that the damage level was estimated based on the percentage of the crushed material as compared to the total volume. The maximum energy absorption for Groups 172 and 288 was 732 J and 1291 J as shown in Table 2. In the meantime, the energy absorption capacity of Groups 318 and 366 could not be properly specified since the specimens did not fully damage under 1123 J and 1357 J impact energies, respectively. The experimental results have shown that the energy absorption capacity increased with the specimen's density. As can be seen that Specimens 366 were able to absorb more impact energy than that of Specimens 288 but the maximum impact forces of these two groups were quite similar (Figs. 12-13). It means that if these two groups are used as a sacrificed layer, the peak impact force transfers from a collision to the protected structures will be similar but the material with ρ = 366 kg/m^3 will be able to absorb more impact energy than those with ρ = 288 kg/m^3.

In order to investigate the impact energy transferred to the load cell, the impact force versus axial displacement curves are presented in Fig. 15. From the figure, it can be seen that Specimen 172 transferred more energy to the load cell. It is noted that this transferring energy is different from the energy absorption and the reason for this observation can be explained as follows. For Specimens 288 and 318, the densification did not occur because of the relatively high density of the specimens and fragmentation of the specimens. As a result, these specimens could not transfer the remaining energy from the projectile to the load cell. On the other hand, the densification in Specimen 172 led to more energy absorption.

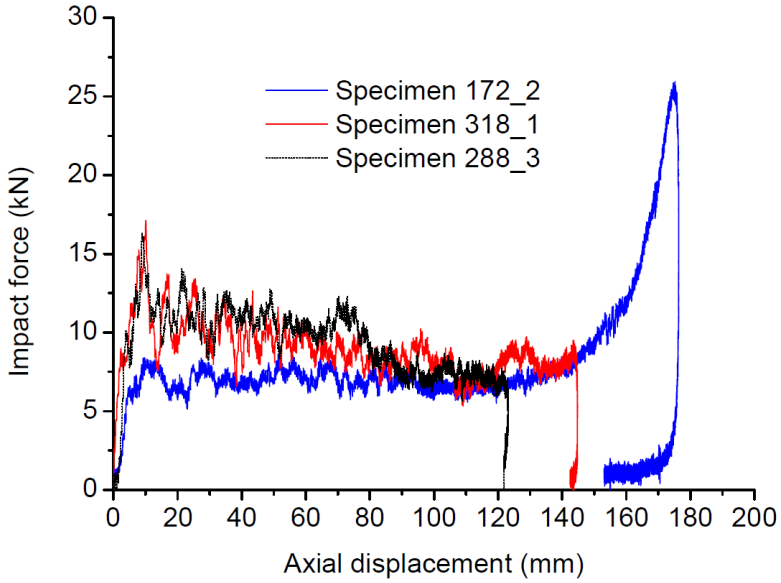

Fig. 15. Impact forces vs axial displacement of the tested specimens

Conclusions

The static/impact response and the energy absorption of the newly developed single phase syntactic foam has been investigated and the following findings can be drawn:

1. The mechanical properties of the syntactic foam including the compressive strength, the yield stress, and the modulus increased with the density but this change slowed down with higher densities.

2. The failure propagation of the tested specimens was dependent on the material density and the impact velocity. The damage of the low-density specimen propagated from the bottom upwards to the top while the damage of the high-density specimen propagated from two ends towards the midheight.

3. A quantitative analysis of the stress evolution in the single phase syntactic foam can be used to predict the progressive failure of the specimens.

4. The densification occurred in low density specimens but did not happen in higher density specimens. Therefore, using high density specimens together with FRP confinement to achieve the densification phenomenon is recommended.

5. The impact energy absorption increased significantly with the density and the wall thickness of the macrospheres.

Finally, the single phase syntactic foam is light and has excellent ability to absorb impact energy. Therefore, this material is recommended for sacrificed layers in protective structures or core layers for composite structures.

Acknowledgement

The support from Australian Research Council via Discovery Early Career Researcher Award (DE160101116) is acknowledged.

References

[1] Gibson L and Ashby M. Cellular solids: structure and properties. Cambridge: Cambridge University Press; 2003.
[2] Gupta N, Zeltmann SE, Shunmugasamy VC, and Pinisetty D. Applications of polymer matrix syntactic foams. JOM. 2014;66(2):245-54.
[3] Lapčík L, Ruszala MJA, Vašina M, Lapčíková B, Vlček J, Rowson NA, Grover LM, and Greenwood RW. Hollow spheres as nanocomposite fillers for aerospace and automotive composite materials applications. Composites Part B: Engineering. 2016;106:74-80.
[4] Kim HS and Oh HH. Manufacturing and impact behavior of syntactic foam. J Appl Polym Sci. 2000;76(8):1324-8.
[5] Altenaiji M, Guan ZW, Cantwell WJ, Zhao Y, and Schleyer GK. Characterisation of aluminium matrix syntactic foams under drop weight impact. Mater Des. 2014;59:296-302.
[6] Durkin S, Fowkes N, Redwood N, and Bassom A. Innovative Approach to Open Pit Edge Protection. In: Proceedings of Ninth AusIMM Open Pit Operators' Conference. Conference, Conference 2016. p. 138–49.
[7] Wu X, Dong L, Zhang F, Zhou Y, Wang L, Wang D, and Yin Y. Preparation and characterization of three phase epoxy syntactic foam filled with carbon fiber reinforced hollow epoxy macrospheres and hollow glass microspheres. Polym Compos. 2016;37(2):497-502.
[8] Le Gall M, Choqueuse D, Le Gac P-Y, Davies P, and Perreux D. Novel mechanical characterization method for deep sea buoyancy material under hydrostatic pressure. Polym Test. 2014;39(Supplement C):36-44.

[9] Pham TM, Kingston J, Strickland G, Chen W, and Hao H. Effect of crumb rubber on mechanical properties of multi-phase syntactic foams. Polym Test. 2018;66:1-12.
[10] Swetha C and Kumar R. Quasi-static uni-axial compression behaviour of hollow glass microspheres/epoxy based syntactic foams. Mater Des. 2011;32(8-9):4152-63.
[11] Geng H, Liu J, Guo A, Ren S, Xu X, and Liu S. Fabrication of heat-resistant syntactic foams through binding hollow glass microspheres with phosphate adhesive. Mater Des. 2016;95:32-8.
[12] Lau K-t, Gu C, and Hui D. A critical review on nanotube and nanotube/nanoclay related polymer composite materials. Composites Part B: Engineering. 2006;37(6):425-36.
[13] Shutov FA. Syntactic polymer foams. Chromatography/Foams/Copolymers: Springer; 1986. p. 63-123.
[14] Colloca M, Gupta N, and Porfiri M. Tensile properties of carbon nanofiber reinforced multiscale syntactic foams. Composites Part B: Engineering. 2013;44(1):584-91.
[15] Zegeye E, Ghamsari AK, and Woldesenbet E. Mechanical properties of graphene platelets reinforced syntactic foams. Composites Part B: Engineering. 2014;60:268-73.
[16] Wu X, Wang Y, Yang X, Yu J, Wang L, Hou S, and Jiang P. A “rolling ball method” to make glass fiber reinforced hollow epoxy macrospheres used for a three phase epoxy syntactic foam. RSC Advances. 2015;5(75):61204-17.
[17] Zhi C, Long H, and Miao M. Microbond testing and finite element simulation of fibre-microballoon-epoxy ternary composites. Polym Test. 2017.
[18] Chen W, Hao H, Hughes D, Shi Y, Cui J, and Li Z-X. Static and dynamic mechanical properties of expanded polystyrene. Mater Des. 2015;69:170-80.
[19] Kim HS and Khamis MA. Fracture and impact behaviours of hollow micro-sphere/epoxy resin composites. Composites Part A: Applied Science and Manufacturing. 2001;32(9):1311-7.
[20] Wouterson EM, Boey FYC, Hu X, and Wong S-C. Fracture and Impact Toughness of Syntactic Foam. Journal of Cellular Plastics. 2004;40(2):145-54.
[21] Maharsia R, Gupta N, and Jerro HD. Investigation of flexural strength properties of rubber and nanoclay reinforced hybrid syntactic foams. Materials Science and Engineering: A. 2006;417(1-2):249-58.
[22] Li G and Jones N. Development of rubberized syntactic foam. Composites Part A: Applied Science and Manufacturing. 2007;38(6):1483-92.
[23] Li G and John M. A crumb rubber modified syntactic foam. Materials Science and Engineering: A. 2008;474(1):390-9.
[24] Song B, Chen WW, and Lu WY. Mechanical characterization at intermediate strain rates for rate effects on an epoxy syntactic foam. International Journal of Mechanical Sciences. 2007;49(12):1336-43.
[25] Li P, Petrinic N, Siviour CR, Froud R, and Reed JM. Strain rate dependent compressive properties of glass microballoon epoxy syntactic foams. Materials Science and Engineering: A. 2009;515(1-2):19-25.
[26] Ouellet S, Cronin D, and Worswick M. Compressive response of polymeric foams under quasi-static, medium and high strain rate conditions. Polym Test. 2006;25(6):731-43.
[27] Peter S and Woldesenbet E. Nanoclay syntactic foam composites—High strain rate properties. Materials Science and Engineering: A. 2008;494(1-2):179-87.
[28] Viot P, Shankar K, and Bernard D. Effect of strain rate and density on dynamic behaviour of syntactic foam. Compos Struct. 2008;86(4):314-27.
[29] Shams A, Panteghini A, Bardella L, and Porfiri M. A micromechanical model to study failure of polymer-glass syntactic foams at high strain rates. Computational Materials Science. 2017;135:189-204.

462 [30] Matrix Engineered. Finely tuned impact absorption.
463 http://www.matrixengineered.com/performance-materials/kinetica-energy-absorption-
464 systems/. Accessed on 09/10/2017
465 [31] He D, Ekere N, and Cai L. Computer simulation of random packing of unequal particles.
466 Physical review E. 1999;60(6):7098.
467 [32] Ashby M. The properties of foams and lattices. Philosophical Transactions of the Royal
468 Society of London A: Mathematical, Physical and Engineering Sciences. 2006;364(1838):15-
469 30.
470 [33] Pham TM and Hao H. Axial impact resistance of FRP-confined concrete. J Compos
471 Constr. 2017;21(2):04016088.
472 [34] Johnson W. Impact strength of materials: Edward Arnold London; 1972.
473 [35] Pham TM, Chen W, and Hao H. Failure and impact resistance analysis of plain and FRP-
474 confined concrete cylinders under axial impact loads. Int J Protect Struct. 2018;9(1):4-23.
475

476 **List of Figures**

492 **List of Tables**

495 Table 1. Experimental results under static loads

Density (kg/m^3)	Yield strain (%)	Yield stress (MPa)	Maximum stress (MPa)	Young's modulus (MPa)	Energy (up to 35% strain) (N.m)
172_1	0.69	0.43	0.62	74.2	36.1
172_2	1.32	0.54	0.63	50.9	37.5
172_3	0.84	0.42	0.61	70.0	35.8
172_4	0.98	0.50	0.58	65.2	34.9
172_5	0.90	0.49	0.63	75.5	36.0
Mean	0.94	0.48	0.61	67.2	36.1
288_1	0.97	1.14	1.36	118.6	70.7
288_2	0.91	1.10	1.30	131.8	69.0
288_3	0.82	1.07	1.34	142.2	70.0
288_4	1.15	1.16	1.34	80.5	66.6
288_5	0.86	0.88	1.24	120.8	65.1
Mean	0.93	1.05	1.30	118.8	67.7
318_1	1.11	1.524	1.76	134.3	106.3
318_2	1.06	1.463	1.67	124.2	99.3
318_3	1.05	1.28	1.71	123.2	99.2
318_4	0.99	1.279	1.68	145.0	101.3
318_5	1.05	1.497	1.75	136.8	106.9
Mean	1.05	1.41	1.71	132.7	103.6
366_1	1.66	2.14	2.27	143.4	132.8
366_2	1.68	1.60	2.26	126.0	131.3
366_3	1.63	2.18	2.24	137.6	131.1
366_4	1.61	1.80	2.23	159.2	128.1
366_5	1.63	1.82	2.32	142.0	133.6
Mean	1.58	1.91	2.26	141.6	131.5

496

497 Table 2. Experimental results of drop-weight impact tests

Specimen	Drop height (m)	Density (kg/m^3)	Impact velocity (m/s)	Residual velocity (m/s)	Energy Absorption (J)	Damage level	Note
172_1	0.63	156	3.57	1.51	523	90%	
172_2	0.95	152	4.39	2.15	732	100%	
172_3	1.29	156	5.06	-0.84	352	minor	28.26 kg projectile
288_1	1.29	226	5.14	0.78	1291	100%	
288_2	0.63	230	3.57	0	637	40%	
288_3	0.95	234	4.34	0	942	80%	
288b_1	1.29	188	5.02	3	813	100%	EPS shrunk
288b_2	0.63	195	3.26	0	531	80%	
318_1	0.95	219	4.47	0	999	90%	EPS shrunk
318_2	0.95	223	4.74	0	1123	80%	
366_1	1.29	269	5.16	0	1331	70%	
366_2	1.29	265	5.21	0	1357	70%	
366_3	0.95	265	4.56	0	1040	<50%	

498